Grain Boundary Microstructural Control through Thermomechanical Processing in a Titanium-Modified Austenitic Stainless Steel

Article *in* Metallurgical and Materials Transactions A · December 2008

DOI: 10.1007/s11661-008-9667-2

CITATIONS
34

READS
222

4 authors:

Sumantra Mandal
Indian Institute of Technology Kharagpur
130 PUBLICATIONS **4,270** CITATIONS
SEE PROFILE

Sivaprasad Palla
SWERIM
86 PUBLICATIONS **1,996** CITATIONS
SEE PROFILE

Baldev Raj
Indira Gandhi Centre for Atomic Research
919 PUBLICATIONS **18,386** CITATIONS
SEE PROFILE

Subramanya Sarma Vadlamani
Indian Institute of Technology Madras
133 PUBLICATIONS **4,150** CITATIONS
SEE PROFILE

Grain Boundary Microstructural Control through Thermomechanical Processing in a Titanium-Modified Austenitic Stainless Steel

SUMANTRA MANDAL, P.V. SIVAPRASAD, BALDEV RAJ, and V. SUBRAMANYA SARMA

The present study discusses the grain boundary microstructural control in a 15Cr-15Ni-2.2Mo-Ti modified austenitic stainless steel (commonly known as alloy D9) through a one-step thermomechanical treatment. The experimental methodology adopted in this investigation was based on the strain annealing approach in which a small amount of strain (5 to 15 pct) was imparted on the solution-annealed (SA) sample. The cold-deformed samples were subsequently annealed at various temperatures (1173 to 1273 K) for different time periods (0.5 to 2 hours). It was observed that annealing after 5 pct deformation induces anomalous grain growth with a moderate increase in number fraction of coincidence site lattice (CSL) boundaries. However, a prestrain of 10 to 15 pct followed by annealing at 1273 K for 0.5 to 2 hours was found to be a suitable thermomechanical processing schedule to increase the number fraction of CSL boundaries (particularly $\Sigma 3$ and its variants) significantly. Further, the well-connected network of random grain boundaries present in the SA specimen was substantially disrupted in these processing conditions due to the incorporation of $\Sigma 3$ and its variants. The preceding results were discussed with reference to strain-induced grain growth *vis-à-vis* strain-induced boundary migration (SIBM) following deformation and annealing.

DOI: 10.1007/s11661-008-9667-2

I. INTRODUCTION

POLYCRYSTALLINE materials have a large number of grain boundaries, and it is well established that the physical, chemical, and mechanical properties of materials are controlled by the number, character, and structure of the boundaries. The concept of "grain boundary design and control" was first introduced by Watanabe in 1984.[1] A few years later, the original concept of grain boundary design was adapted to improve the intergranular corrosion resistance of face-centered-cubic (fcc) materials,[2] and the topic has evolved into "grain boundary engineering (GBE)." The central point of GBE is to optimize the grain boundary character distribution (GBCD) by increasing the proportion of "special" low energy boundaries, because they were shown to exhibit increased resistance to creep,[3] fatigue,[4] fracture,[5] intergranular degradation,[6] as well as better weldability and service performance.[7]

Special boundaries (SBs) are those that have better properties than average or random high-angle boundaries (HABs). The SBs shows better properties because they have higher atomic ordering and lower energy and are often described in terms of the coincidence site lattice (CSL) model.[8] The CSL boundaries are characterized by a certain axis and angle of misorientation, which allow atoms from neighboring lattices to notionally coincide, and the reciprocal density of coinciding sites is designated as Σ. It is well established that SBs are those with CSL values up to 29. The GBCD optimization therefore requires an enhancement in SBs ($\Sigma \leq 29$), so that connectivity of HABs could be broken significantly. In GBCD manipulation, special attention is given to the twin ($\Sigma 3$) and its variants ($\Sigma 3^n$) and is also termed as twin-induced GBE. Because fcc metals with low stacking fault energy show prolific twinning during thermomechanical processing, the GBE research has been centered mainly on these classes of materials.

Thermomechanical processing, through a sequence (single step or iterative) of strain and recrystallization or annealing treatments, has been shown to be effective in achieving optimized GBCD in different fcc metals and alloys.[9] Iterative strain recrystallization involves higher levels of strain (typically 20 to 30 pct) followed by short annealing for a few minutes at a temperature of 0.6 to $0.8T_m$ to induce partial recrystallization in each cycle. Schwartz *et al.*[10] have used a strain-recrystallization approach on alloy IN600 bar material with 20 pct reductions per pass (up to seven passes) and annealing at 1273 K for 7 minutes. Iterative strain annealing, on the other hand, involves a small amount of strain (typically <7 pct) followed by annealing for many hours at temperatures typically below those used for recrystallization.[11] Though iterative processing has been found to

SUMANTRA MANDAL and P.V. SIVAPRASAD, Scientific Officers, and BALDEV RAJ, Director, are with the Metallurgy and Materials Group, IGCAR, Kalpakkam, TN-603102, India. Contact e-mail: sumantra@igcar.gov.in V. SUBRAMANYA SARMA, Assistant Professor, is with the Department of Metallurgical and Materials Engineering, IIT Madras, TN-600036, India.

Manuscript submitted February 9, 2008.
Article published online October 28, 2008

be quite effective in increasing the proportion of Σ3 boundaries, the simpler one-step process would be suitable for industrial applications. For example, Michiuchi *et al.* have suggested a one-step thermomechanical processing for 316 austenitic stainless steel (3 pct strain and annealing at 1240 K for 72 hours), and this increased the CSL fraction to 86 pct as compared to 56 pct in the as-received condition.[12] Shimada *et al.* have adopted an almost similar processing schedule for 304 austenitic stainless steel (5 pct strain and annealing at 1200 K for 72 hours), which improved the CSL frequency to 87 pct as compared to 63 pct in the starting material.[13] Though the aforementioned processing schedules could be easily implemented in industry, the longer annealing time would decrease the production rate and increase the production cost. Further, longer annealing times would invoke significant grain growth in the final microstructure, which could be detrimental to the mechanical properties.

The objective of the present research is to design a one-step thermomechanical processing schedule in a 15Cr-15Ni-2.2Mo-Ti modified austenitic stainless steel (commonly known as alloy D9) to produce an optimum microstructure for development of a high performance corrosion resistance austenitic stainless steel. The present study attempts to understand and evaluate the influence of "prestrain–annealing temperature–annealing time" parameters on the GBCD, which in turn would help to understand the micromechanisms involved in the grain boundary microstructure control of alloy D9.

II. EXPERIMENTAL

The alloy D9 used in the present investigation was supplied by M/s. MIDHANI (Hyderabad, India), in the solution-annealed (SA) condition. The chemical composition of the alloy is given in Table I. The SA specimens were subjected to cold rolling and annealing. The experimental variables chosen for this investigation were as follows: (1) extent of prestrain by cold rolling, (2) annealing temperature, and (3) annealing time. Cold rolling operations were carried out on 3-mm-thick rectangular plates on a laboratory rolling mill. The extent of deformation employed in this study was 5, 10, and 15 pct, respectively. Subsequently, deformed specimens were annealed in vacuum-sealed quartz capsules at three different temperatures (1173, 1223, and 1273 K) for three different periods of time (30 minutes, 1 hour, and 2 hours). The heat-treated specimens were quenched in cold water. Table II summarizes the combinations of thermomechanical processing conditions adopted in the present study.

Sections from the processed strip were cut and polished to 1 μm using the standard metallographic polishing procedure. Samples were further polished using 0.04-μm colloidal silica to ensure removal of any residual surface deformation. Electron backscatter diffraction (EBSD)–based orientation imaging microscopy (OIM) scans were performed on all the processed samples to determine the GBCD in the materials using a TSL-OIM system on a FEI Quanta 200 scanning electron microscope operating at 30 kV. The OIM maps were collected from the samples using a step size of 1 to 2 μm depending on the grain size. The grain boundary character was defined as follows. Low angle or Σ1 boundaries were defined as those with misorientations (θ) 5 deg $< \theta \leq$ 15 deg. Boundaries with 2 deg $< \theta \leq$ 5 deg misorientations were considered as sub-boundaries. For identifying CSL boundaries,[14] Brandon's criterion[15] was used. The maximum deviation angle $\Delta\theta_C$, which can be accommodated in a Σ boundary by introducing grain boundary structural dislocations, according to this criterion is given by $\Delta\theta_C = 15\Sigma^{-1/2}$, in degrees. Random HABs are defined as those with misorientations >15 deg and that are not low Σ (Σ ≤ 29) CSL boundaries. To ensure statistical significance, averaged values of GBCD were calculated based on three maps (each of 500 μm × 500 μm) obtained from different areas in each sample covering over 1000 grains.

III. RESULTS

A. *As-Received Microstructure*

The microstructure of the as-received material is shown in Figure 1. The mean linear intercept grain size value is 18 μm. The grain boundaries are identified as one of the following categories: Σ1, Σ3, Σ9, Σ27, and other low Σ CSL or random HABs. The as-received material contained 45 pct of Σ3 boundaries. The GBCD data reported in this article were determined on the basis of number fraction. A close look on Figure 1 reveals that Σ3 boundaries have straight and parallel morphology. Twins are present in both the large and small grains, which indicates that the twins were generated during the recrystallization and grain growth stages.[9] The proportions of Σ1, Σ9, and Σ27 boundaries are 3.5, 2.9, and 0.8 pct, respectively. The total percentage of

Table II. Thermomechanical Processing Conditions for Alloy D9 Adopted in the Present Study

Strain (Pct)	Annealing Temperature (K)	Annealing Time (h)	Sample Number*
5	1173, 1223, 1273	0.5 , 1, 2	R5–*x* K–*y* h
10	1173, 1223, 1273	0.5 , 1, 2	R10–*x* K–*y* h
15	1173, 1223, 1273	0.5 , 1, 2	R15–*x* K–*y* h

*In the sample number, *x* stands for the annealing temperature and *y* for the annealing time period.

Table I. Chemical Composition (Weight Percent) of 15Cr-15Ni-2.2Mo-Ti Modified Austenitic Stainless Steel (Alloy D9)

C	Mn	Si	S	P	Cr	Ni	Mo	Ti	B	Co	N
0.052	1.509	0.505	0.002	0.011	15.051	15.068	2.248	0.21	0.001	0.01	0.006

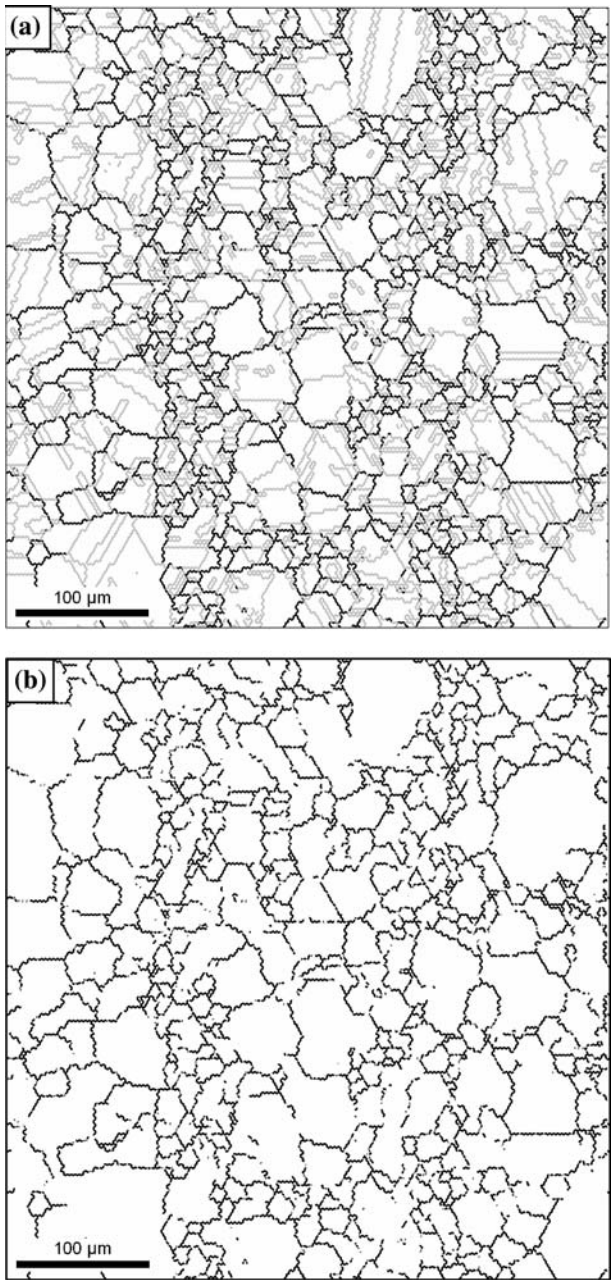

Fig. 1—Microstructure of the SA sample. (*a*) Grain boundary reconstruction from EBSD data, the thick black and thin gray lines represent random HABs and SBs, respectively. (*b*) Only random HABs are shown to assess the random boundary connectivity.

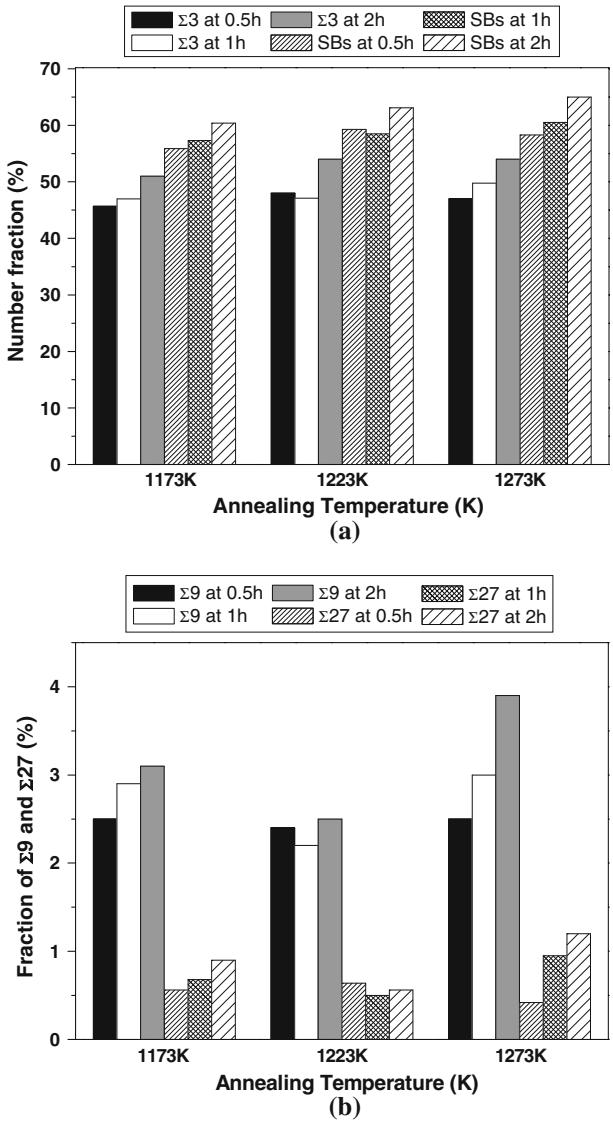

Fig. 2—Influence of annealing temperature and time on (*a*) Σ3 and SBs and (*b*) Σ9 and Σ27 boundaries at 5 pct deformation level.

SBs in the as-received specimen is ~55 pct. It should be noted that SBs in this article refer to CSL boundaries with $\Sigma \leq 29$. Figure 1(b) shows only the random HABs in the as-received sample. It could be seen that the random HABs are well connected and provide a potential path for percolation (Figure 1(b)).

B. *Annealing with 5 Pct Prestrain*

The GBCD data in terms of CSL boundaries for samples annealed in the temperature range 1173 to 1273 K with 5 pct prestrain are shown in Figure 2. The fraction of Σ3 boundaries and SBs are shown in Figure 2(a), and the Σ9 and Σ27 fractions are shown in Figure 2(b). It is seen that annealing following 5 pct deformation results only in a moderate increase in proportion of SBs as well as twins (Σ3 and its variants). The maximum proportion of SBs with 5 pct prestrain was observed after annealing at 1273 K for 2 hours. The proportion of SBs in this condition has increased to 65 pct from the 55 pct in as-received specimen. The corresponding Σ3 boundaries are about 54 pct as compared to 45 pct in the SA specimen. The proportion of Σ1 boundary has decreased to 2.1 pct from 3.5 pct in the SA specimen. Figure 3 shows the typical microstructure obtained following the 5 pct prestrain and annealing. It is clear that anomalous grain growth has occurred, resulting in a bimodal grain size distribution consisting of very large and very small grains. The HABs shown in Figure 3(b) reveal that a considerable

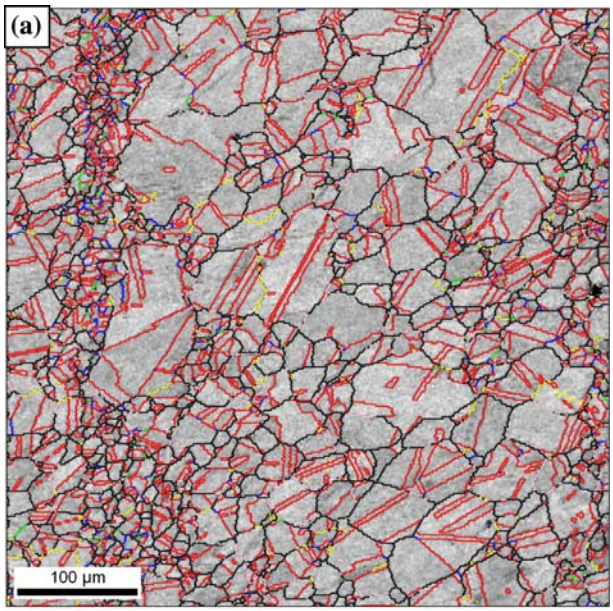

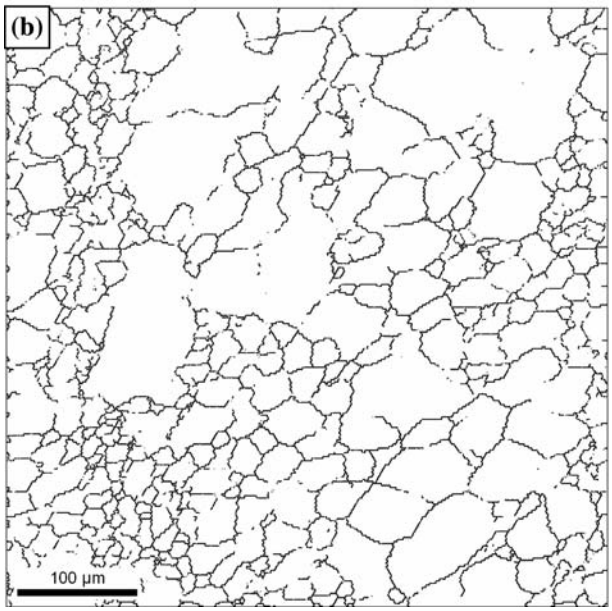

Fig. 3—(*a*) OIM map of the sample R5–1273 K–1 h (color code: Σ3—red; Σ9—blue; Σ27—green; Σ1—yellow; other low Σ CSL—purple, and random HABs—black). (*b*) Grain boundary map showing only the random HABs.

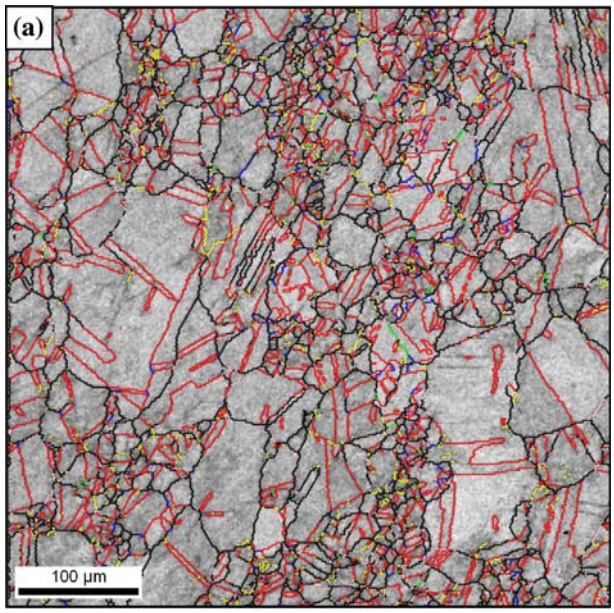

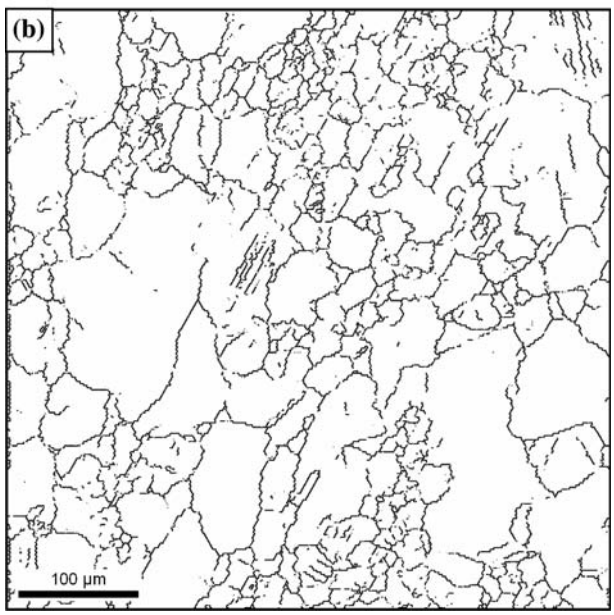

Fig. 4—(*a*) OIM map of the sample R15–1173 K–1 h (color code is the same as that of Fig. 3). (*b*) Grain boundary map showing only the random HABs.

amount of random HAB clusters with significant connectivity still exist in the microstructure.

C. *Annealing with 10 to 15 Pct Prestrain*

The microstructural evolution of the samples annealed in the temperature range 1173 to 1273 K with 10 to 15 pct prestrain was found to be rather complex. The representative microstructure after annealing at 1173 K with 15 pct prestrain is shown in Figure 4. Annealing at 1173 K for 1 hour resulted in anomalous grain growth (Figure 4). The EBSD reconstructed grain boundary map (Figure 4(b)) shows only a marginal improvement in random HAB cluster fragmentation. A significant difference in appearance of the microstructure was observed after annealing at 1273 K for 1 hour (Figure 5). It was observed that anomalous grain growth did not occur. The grain boundary network has been extensively modified by Σ3 boundaries. The morphology of Σ3 is mainly convoluted. In fact, it is very difficult to define a "grain" and quantitatively measure "grain size" in a microstructure, where the grain boundary network is considerably fragmented with twin boundaries.[16] The random HAB map shown in Figure 5(b) reveals a significant disruption of random boundary connectivity due to direct incorporation of Σ3 and its variants.

The GBCD data in terms of CSL boundaries in samples annealed in the temperature range 1173 to

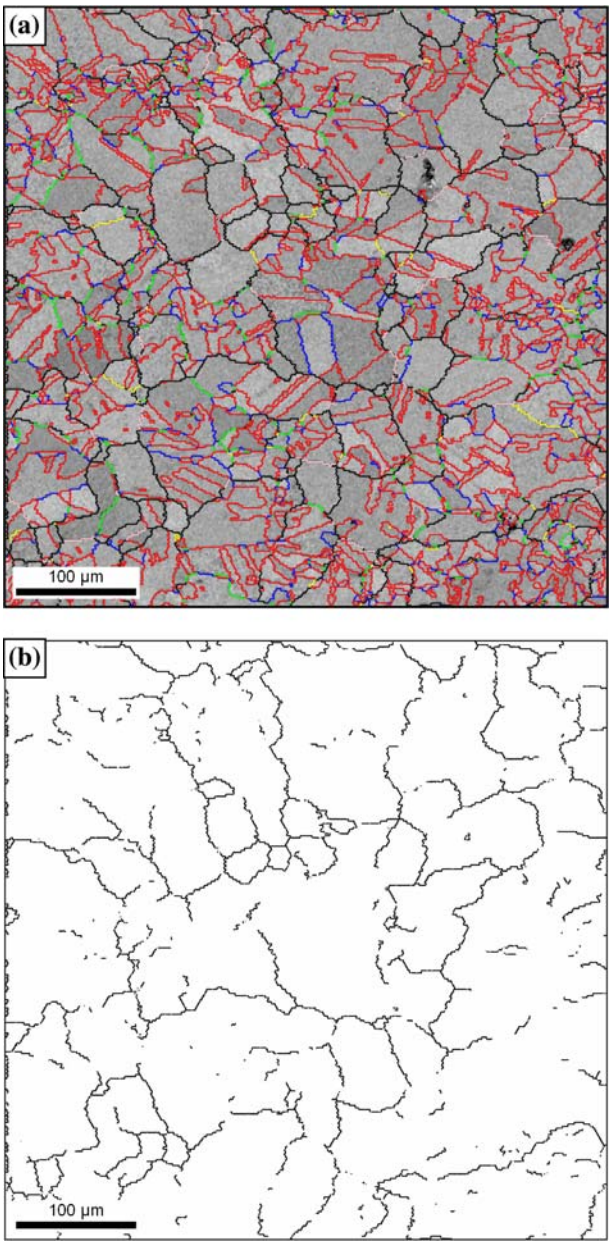

Fig. 5—(*a*) OIM map of the sample R15–1273 K–1 h (color code is the same as that of Figure 3). (*b*) Grain boundary map showing only the random HABs.

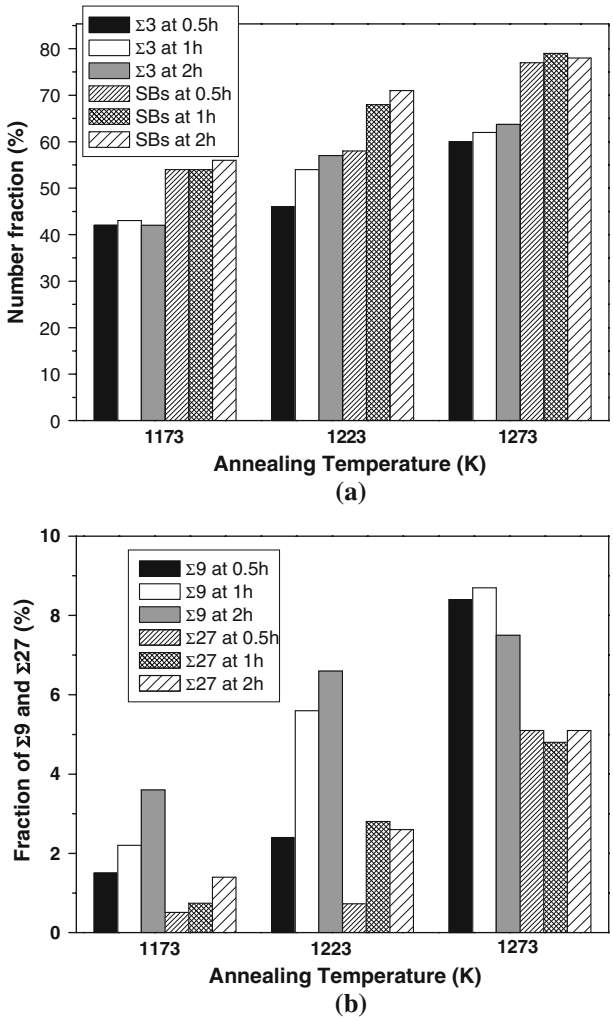

Fig. 6—Influence of annealing temperature and time on (*a*) Σ3 and SBs and (*b*) Σ9 and Σ27 boundaries at 15 pct deformation level.

1273 K with 15 pct prestrain are shown in Figure 6. (The 10 pct deformed specimen showed an almost similar trend as the 15 pct prestrained sample and therefore is not emphasized here). It could be observed that no improvement in terms of Σ3 proportion was observed at 1173 K (Figure 6(a)). Rather, the percentage of Σ3 boundaries has decreased marginally to 42.5 pct in R15–1173 K–1 h as compared to 45 pct in the SA sample. The Σ1 proportion, on the other hand, has increased to 5.3 pct. The total percentage of SBs in this sample is 54 pct. However, a notable increase in Σ3 and SBs fraction was observed at 1273 K. The fraction of higher order twin boundaries (*i.e.*, Σ9 and Σ27) has also substantially increased following annealing at 1273 K (Figure 6(b)). The maximum (~79 pct) proportions of SBs have been obtained in the sample R15–1273 K–1 h. The frequencies of Σ3, Σ9, and Σ27 boundaries are 62, 8.7, and 4.7 pct, respectively. The proportion of Σ1 boundary, in this condition, is only 1.25 pct.

IV. DISCUSSION

It was observed in the present study that annealing with 5 pct prestrain resulted in anomalous grain growth in alloy D9. Anomalous grain growth has also been observed in Ni annealed at 1273 K with 2 pct prestrain[17] as well as in type 316 stainless steel annealed at 1198 K with 3 pct prestrain.[9] The anomalous grain growth in alloy D9 could be attributed to the so-called "strain-induced grain growth." It has been shown that residual dislocations could be present even after primary recrystallization is complete.[18] Further, annihilation of dislocations during primary recrystallization leaves behind inhomogeneously distributed elastic strains.[19] In essence, the SA sample may contain inhomogeneously distributed local strain after recrystallization.

When the SA sample is subjected to a low level of strain, nonequilibrium extrinsic grain boundary dislocations (EGBDs) may be generated,[17] which in turn are annihilated by climb during heat treatment. The strain field associated with EGBDs enhances the migration properties of grain boundaries under the thermal driving force during annealing. Pumphrey and Gleiter[20] have shown that, during annihilation of EGBDs, grain boundary movement occurs. Because the rate of migration depends upon local strain, intrinsic boundary mobility, and grain boundary curvature, some grains grow rapidly while the others do not. This leads to abnormal grain growth, as shown in Figure 3. Because twinning occurs during the grain growth process,[21] there is a moderate increase in Σ3 boundaries in these processing conditions (Figure 2(a)) as compared to the SA specimen. Further, interactions between boundaries that may generate higher order twin boundaries seem to occur (to a lesser extent) in these processing conditions. For example, the fraction of (Σ9 + Σ27) boundaries was ~5 pct in the R5–1273 K–2 h (Figure 2(b)) specimen as compared to 3.7 pct in the SA sample.

In the present investigation, the GBE microstructure was achieved only after annealing at 1273 K with 10 to 15 pct deformation. A dramatic change in GBCD was observed in the 15 pct prestrained sample when the annealing temperature was raised to 1273 K from 1173 K (Figure 6). The increase in the annealing temperature has resulted in a substantial increase in Σ3 fraction from 44 pct in R15–1173 K–1 h to 62 pct in R15–1273 K–1 h. The fraction of (Σ9 + Σ27) boundaries in the sample R15–1273 K–1 h has also increased to 13.5 pct when compared to the value of 2.9 pct in R15–1173 K–1 h. The increase in Σ3 and its variants (*i.e.*, $\Sigma 3^n$) in the sample R15–1273 K–1 h signifies extensive twin interactions.[11] On the other hand, a lower amount of $\Sigma 3^n$ fractions in the R15–1173 K–1 h sample indicates fewer interactions between twin boundaries. The fraction of $\Sigma 3^n$ boundaries R15–1173 K–1 h is lower than that of the starting material. This could be attributed to the loss of twin orientation due to deformation. This could be substantiated from Figure 7, which illustrates the deviation of Σ3 and Σ9 boundaries from the ideal orientation. It could be observed that the majority of Σ3 and Σ9 boundaries in the as-received samples are within 2 deg from their ideal orientation (Figure 7(a)). However, a significant deviation toward higher angle can be seen in the R15–1173 K–1 h specimen (Figure 7(b)). It should be noted here that the deviation of Σ3 and Σ9 boundaries in the R15–1273 K–1 h specimen is found to be within 2 deg.

Now the question is what causes such differences in the microstructure in these two samples as far as the GBCD is concerned. To understand this, misorientation distribution plots in the two samples are analyzed. The absence of a definite peak (Figure 8(a)) at 40 deg (Σ9/38.9⟨111⟩) and 60 deg (Σ3/60⟨111⟩) signifies the loss of twin orientation, as discussed previously. It could be observed that a large fraction of low-angle sub-boundaries (<5 deg) are present in the sample R15–1173 K–1 h (Figure 8(a)). To illustrate the distribution of these low-angle sub-boundaries, an OIM map of this

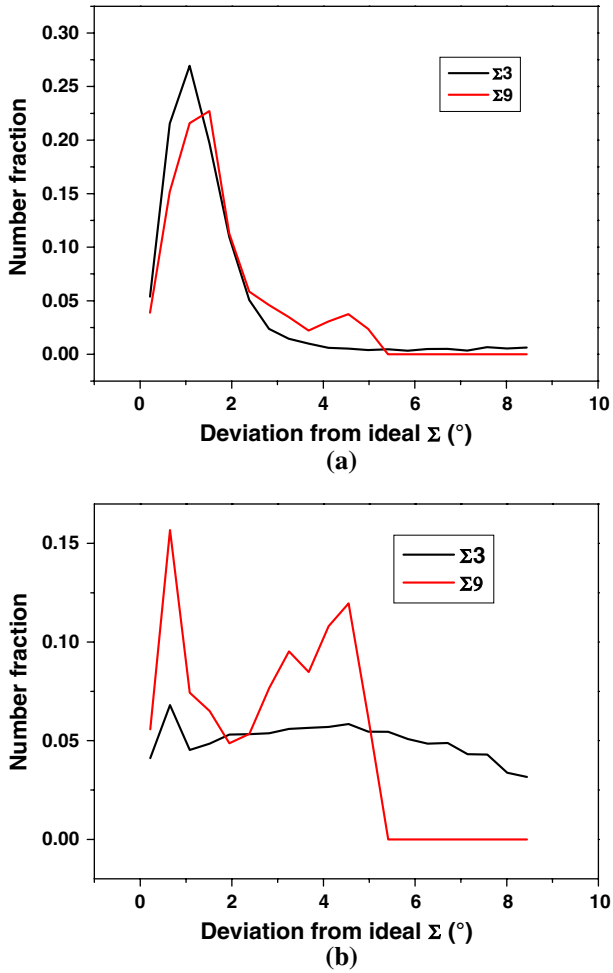

Fig. 7—Deviation of Σ3 and Σ9 boundaries from its ideal orientation in (*a*) SA sample (numbers of Σ3 and Σ9 boundaries studied are 16,592 and 863, respectively) and (*b*) R15–1173 K–1 h specimen (numbers of Σ3 and Σ9 boundaries studied are 11,248 and 708, respectively).

specimen is shown in Figure 8(b). By comparing Figures 4(a) and 8(b), one can see that most of the boundaries with 2 to 5 deg misorientation (*i.e.*, sub-boundaries and accumulated dislocations) do not take part in the grain boundary network and thereby do not contribute to the breakup of the random HAB connectivity. Therefore, they should not be considered as SBs (though they have very low energy due to small misorientation), and considering them as low-angle boundaries will overestimate the proportion of Σ1 boundaries. The presence of sub-boundaries with 2 to 5 deg misorientation could be inferred as an indication of the retained strain within grains. The presence of retained strain is apparent predominantly within the smaller grains (Figure 8(b)), indicating that the dislocations accumulated during cold rolling were not consumed during annealing. Though the microstructural appearance in R15–1173 K–1 h (Figure 4) looks similar to that of R5–1273 K–1 h (Figure 3), the underlying mechanism responsible for the microstructure is believed to be different. The migration of grain boundaries due to

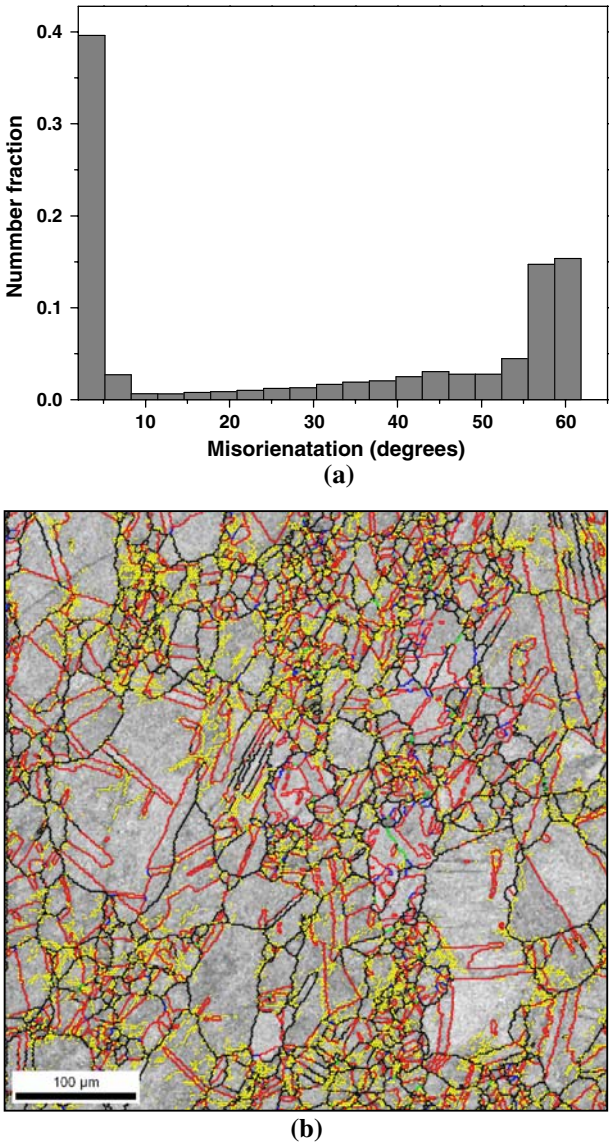

Fig. 8—(*a*) Misorientation distribution plot of the sample R15–1173 K–1 h and (*b*) OIM map where grain boundaries with misorientation >2 deg were considered (color code is the same as that of Figure 3).

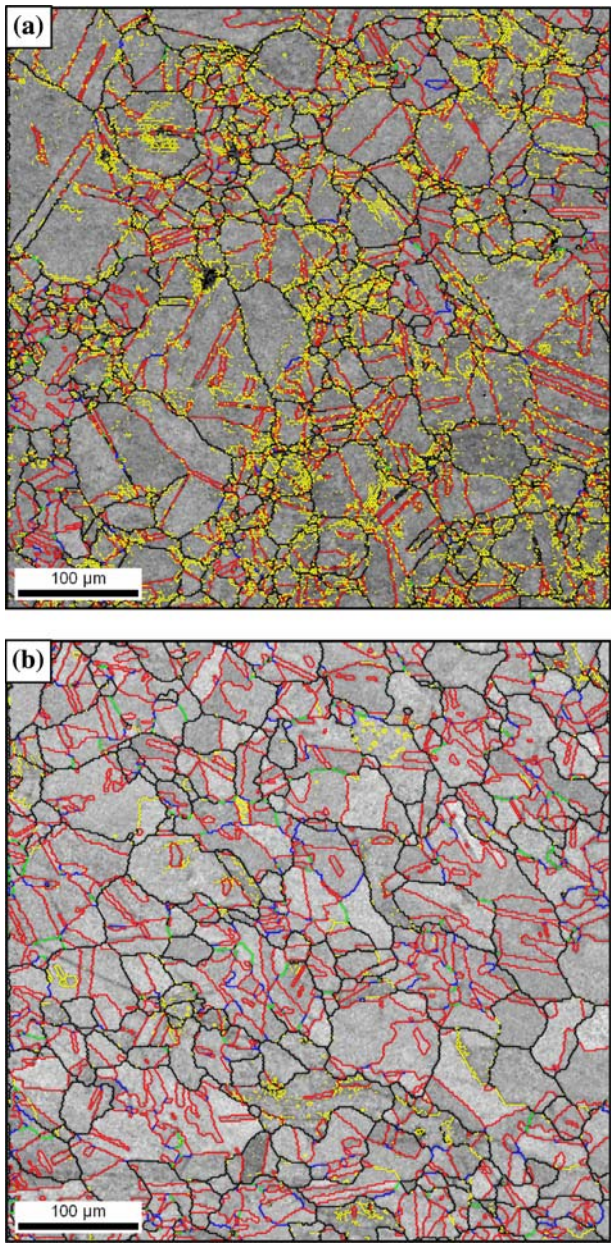

Fig. 9—OIM map of the sample (*a*) R15–1223 K–0.5 h and (*b*) R15–1223 K–1 h where grain boundaries with misorientations >2 deg were considered (color code is the same as that of Figure 3).

annihilation of EGBDs may not be predominant in R15–1173 K–1 h, because deformation of the order of 10 to 15 pct would lead to hardening throughout the grain.[22] Under such conditions, SIBM due to local variation in the stored energy would occur if the thermal driving force (*i.e.*, annealing temperature and time) is sufficient enough. The preferential consumption of accumulated dislocations and propensity toward selective grain boundary migration in R15–1173 K–1 h is attributed to the intrinsic boundary mobility coupled with lower thermal driving force. At longer annealing times, elimination of accumulated dislocations due to SIBM was found to occur to a large extent (Figure 9). The presence of retained strain is obvious in the sample R15–1223 K–0.5 h (Figure 9(a)), whereas the R15–1223 K–1 h sample reveals much lower retained strain (Figure 9(b)). On the other hand, samples annealed at 1273 K contain very negligible proportions of low-angle boundaries (Figure 10), indicating the absence of retained strain. This further suggests that the thermal driving force in these conditions is sufficient enough to consume all the dislocation accumulated during cold rolling. The evolution of microstructure in these samples could be understood as follows. The combined strain and thermal energy is insufficient to trigger recrystallization.[23] However, the density of lattice dislocations is sufficient enough to promote SIBM. In this condition, grain boundary moves at an optimal rate, which is ideal for twin multiplication. During SIBM, interaction between two pre-existing twins occurs frequently, resulting in a Σ9 boundary according to the relationship

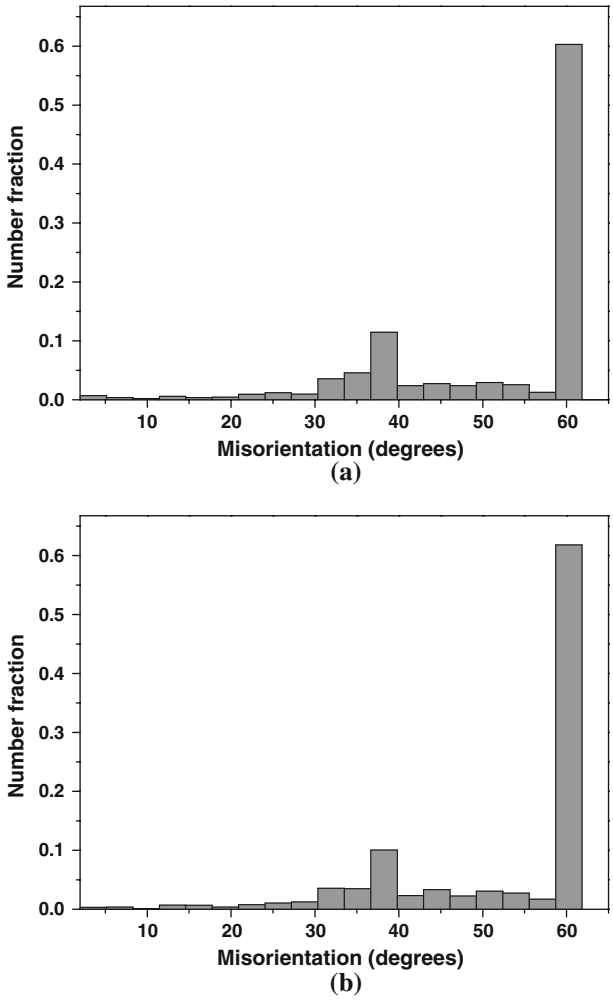

Fig. 10—Misorientation distribution plot of the sample (*a*) R15–1273 K–0.5 h and (*b*) R15–1273 K–1 h.

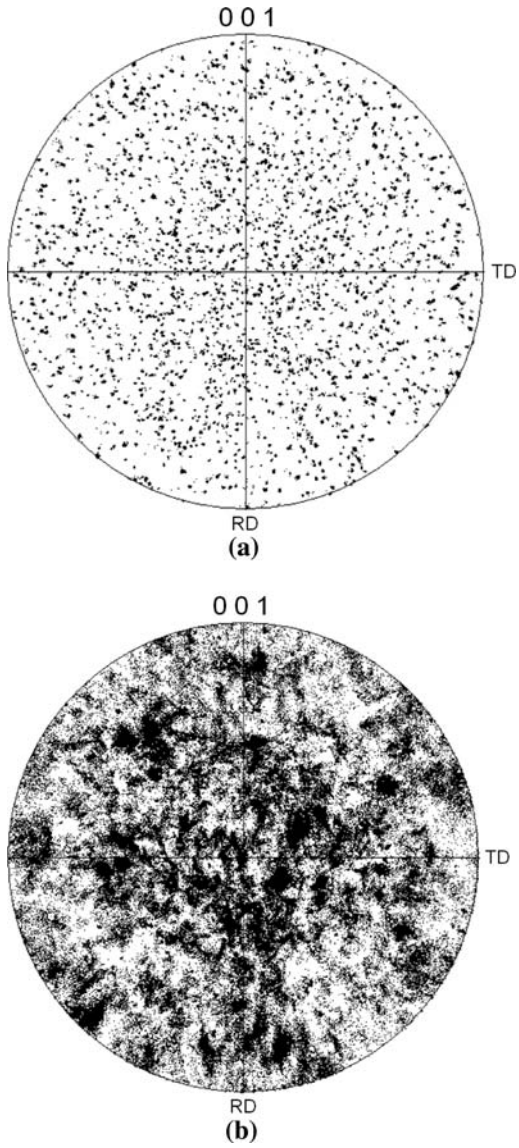

Fig. 11—{100} pole figure of the specimen (*a*) R15–1273 K–1 h and (*b*) R15–1173 K–1 h.

$\Sigma 3 + \Sigma 3 = \Sigma 9$.[24] When a $\Sigma 9$ generated in this way encounters another $\Sigma 3$ in the microstructure, either a new $\Sigma 3$ or a $\Sigma 27$ results according to $\Sigma 3 + \Sigma 9 = \Sigma 3$ or $\Sigma 3 + \Sigma 9 = \Sigma 27$. However, from the statistics of the $\Sigma 3$, $\Sigma 9$, and $\Sigma 27$, as described previously, it could be inferred that $\Sigma 3 + \Sigma 9 = \Sigma 3$ occurs more frequently than $\Sigma 3 + \Sigma 9 = \Sigma 27$. This has also been categorized as the "$\Sigma 3$ regeneration mechanism," which states that $\Sigma 3^n + \Sigma 3^{n+1} = \Sigma 3$ occurs predominantly at triple junctions than $\Sigma 3^n + \Sigma 3^{n+1} = \Sigma 3^{n+2}$.[16,25] This mechanism also predicts that regenerated $\Sigma 3$ in this way will be incoherent; or, in other words, if the $\Sigma 3$ regeneration mechanism operates, the microstructure will contain a large fraction of incoherent twins. With the advancement of the EBSD technique, it is now possible to differentiate between coherent and incoherent twin boundaries with the single section trace analysis[26] or five parameter assessments.[27] In these analyses, it has been shown that straight $\Sigma 3$ boundaries are likely to be coherent twins, whereas curved ones are definitely incoherent. The convoluted topography of several $\Sigma 3$ boundaries in the R15–1273 K–1 h (Figure 5) sample confirms the presence of incoherent twin boundaries. On the other hand, straight and parallel appearance of $\Sigma 3$ boundaries in the R15–1173 K–1 h sample (Figure 4) indicates that the majority of $\Sigma 3$ boundaries are coherent. This fits well with the preceding postulation that significant twin interactions due to SIBM occurred in the sample R15–1273 K–1 h that led to the formation of incoherent twins, whereas very few such interactions occurred in the sample R15–1173 K–1 h. The occurrence of multiple twinning in the sample R15–1273 K–1 h could also be supported from the fact that the resulting texture in this condition is almost random (Figure 11(a)). Because multiple twinning significantly increases the number of texture variants, the resulting texture is almost random. In contrast, a moderate texture is seen in the sample R15–1173 K–1 h (Figure 11(b)), which rules out the possibility of significant twinning in this condition.

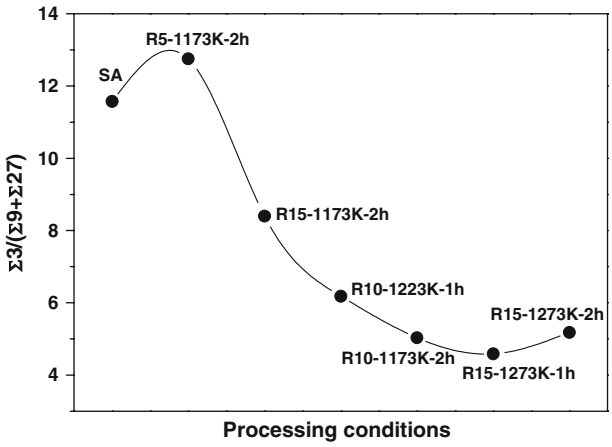

Fig. 12—Ratio of Σ3 to (Σ9 + Σ27) in various processing conditions.

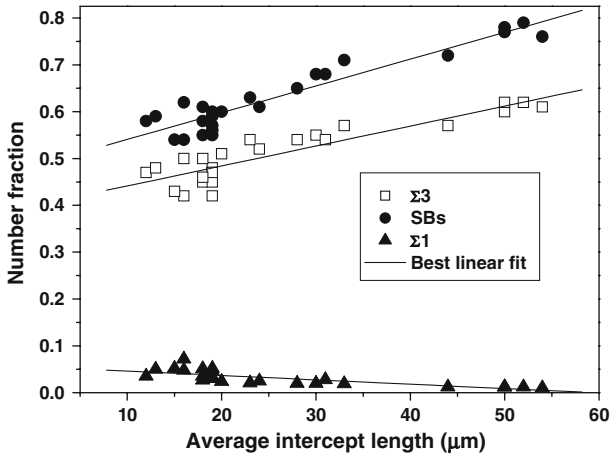

Fig. 13—Correlation between GBCD and grain size during GBE in alloy D9.

Though increasing the proportions of Σ3 boundaries is central to GBE practice, a higher proportion of Σ3 is not necessarily the absolute criterion to achieve GBE material. This view stems from the fact that the number fraction of Σ3 boundaries in various GBE materials is found to vary between 22 and 67 pct.[16] Because Σ9 and Σ27 boundaries are usually generated by multiple twinning, the ratio of Σ3 to (Σ9 + Σ27) would reveal the efficiency of multiple twinning. Further, as effective disruption of the random boundary connectivity occurs with the introduction of Σ3-Σ3-Σ9 or Σ3-Σ9-Σ27 triple junctions, the ratio of Σ3 to (Σ9 + Σ27) would provide better indication toward fragmentation of random HAB networks. In this context, Σ9 is a key element for GBE, because it acts as a bridging segment between Σ3 boundaries.[11] The ratio Σ3 to (Σ9 + Σ27) for various thermomechanically processed samples is shown in Figure 12. It could be observed that the ratio decreases from 11.57 in the SA sample to 4.59 in the sample R15–1273 K–1 h. This clearly signifies a significant interaction between $\Sigma 3^n$ boundaries, which, in turn, break up the random boundary connectivity. It should be noted that the reported value of Σ3/(Σ9 + Σ27) in various GBE materials lies in the range of 1.8 to 6.7.[16]

A. *GBCD and Grain Size*

The relation between GBCD and grain size is not well established. An inverse correlation has been observed between CSL frequency and grain size for polycrystalline materials with fcc and body-centered cubic materials having high stacking fault energy.[28] In the case of austenitic stainless steel having low stacking fault energy, the CSL frequency was found to increase with increasing grain size.[29] Interestingly, no definite correlation between CSL frequency and grain size was observed in the previous work.[30] To clarify this point, the relationship between GBCD and grain size was investigated in this study. It was observed that both the CSL and Σ3 boundary fractions increased with grain size (Figure 13). This increase in grain size is due to SIBM, as discussed previously. Because recrystallization has not been initiated, the grain boundary migration results in an increase in the grain size in the product microstructure. The associated grain growth during GBCD optimization has been reported in many low to medium stacking fault energy materials.[31,32] This signifies that some grain growth is always associated with GBE, at least in the case of low to medium stacking fault energy materials, whereas increase in CSL frequency is primarily due to Σ3 twin boundaries. Figure 13 also reveals that the fraction of Σ1 boundaries decreases with the increase in fraction of Σ3 boundaries. A similar finding was also reported in Reference 33. This decrease in Σ1 boundary fraction with multiple twinning is due to randomization of texture (Figure 11(a)).[34]

V. CONCLUSIONS

The thermomechanical processing schedule and possible micromechanism of twinning related GBE in a Ti-modified austenitic stainless steel (commonly known as alloy D9) has been discussed. A one-step thermomechanical treatment has been adopted in this study in which a small amount of strain (5 to 15 pct) was imparted on the SA sample. The cold-deformed samples were subsequently annealed at various temperatures (1173 to 1273 K) for different time periods (0.5 to 2 hours). It was observed that annealing at 1173 to 1273 K after 5 pct deformation induces anomalous grain growth with a moderate increase in the number fraction of Σ3 boundaries and its variants. This was attributed to the migration of grain boundaries due to the annihilation of EGBDs. A significant improvement in the number fraction of CSL boundaries (particularly Σ3 and its variants) was obtained after annealing at 1273 K with 10 to 15 pct prestrain. The well-connected network of random grain boundaries present in the SA specimen was substantially disrupted in these processing conditions due to incorporation of Σ3 and its variants. This increase in Σ3 and its variants and the resulting disruption of random boundary connectivity were attributed to the occurrence of multiple twinning events. Study of the relation between GBCD and grain size

showed that the CSL and Σ3 boundary fractions increased with grain size. A 10 to 15 pct strain followed by annealing at 1273 K for 0.5 to 2 hours was found to be a suitable thermomechanical processing schedule to produce the GBE microstructure in alloy D9.

REFERENCES

1. T. Watanabe: *Res. Mech.*, 1984, vol. 11, pp. 47–84.
2. G. Palumbo, P.J. King, K.T. Aust, U. Erb, and P.C. Lichtenberger: *Scripta Metall. Mater.*, 1991, vol. 25, pp. 1775–80.
3. T. Watanabe: *Mater. Sci. Eng. A*, 1993, vol. 166, pp. 11–28.
4. U. Krupp, P.E.-G. Wagenhuber, W.M. Kane, and C.J. McMahon, Jr.: *Mater. Sci. Technol.*, 2005, vol. 21, pp. 1247–54.
5. T. Watanabe, S. Tsurekawa, S. Kobayashi, and S. Yamaura: *Mater. Sci. Eng. A*, 2005, vols. 410–411, pp. 140–47.
6. P. Lin, G. Palumbo, U. Erb, and K.T. Aust: *Scripta Metall. Mater.*, 1995, vol. 33, pp. 1387–92.
7. E.M. Lehockey, G. Palumbo, and P. Lin: *Metall. Mater. Trans. A*, 1998, vol. 29A, pp. 3069–79.
8. D.H. Warrington and M. Boon: *Acta Metall. Mater.*, 1975, vol. 23, pp. 599–607.
9. G. Owen and V. Randle: *Scripta Mater.*, 2006, vol. 55, pp. 959–62.
10. A.J. Schwartz, M. Kumar, and W.E. King: *MRS Symposium Proceedings*, Materials Research Society, Pittsburgh, PA, 2000, vol. 586, pp. 3–14.
11. V. Randle: *Acta Mater.*, 2004, vol. 52, pp. 4067–81.
12. M. Michiuchi, H. Kokawa, Z.J. Wang, Y.S. Sato, and K. Sakai: *Acta Mater.*, 2006, vol. 54, pp. 5179–84.
13. M. Shimada, H. Kokawa, Z.J. Wang, Y.S. Sato, and I. Karibe: *Acta Mater.*, 2002, vol. 50, pp. 2331–41.
14. M. Kronberg and F.H. Wilson: *Trans. AIME*, 1949, vol. 185, pp. 501–17.
15. D.G. Brandon: *Acta Metall.*, 1966, vol. 14, pp. 1479–84.
16. V. Randle and G. Owen: *Acta Mater.*, 2006, vol. 54, pp. 1777–83.
17. V. Randle: *Phil. Mag. A*, 1993, vol. 67, pp. 1301–13.
18. V. Randle: *Metall. Trans. A*, 1990, vol. 21A, pp. 2215–21.
19. D.J. Srolovitz, G.S. Grest, and M.P. Anderson: *Acta Metall.*, 1985, vol. 33, pp. 2233–47.
20. P. Pumphrey and H. Gleiter: *Phil. Mag.*, 1971, vol. 35, pp. 365–70.
21. C.S. Pande, M.A. Imam, and B.B. Rath: *Metall. Trans. A*, 1990, vol. 21A, pp. 2891–96.
22. B.M. Guyot and N.L. Richards: *Mater. Sci. Eng. A*, 2005, vol. 395, pp. 87–97.
23. M. Kumar, A.J. Schwartz, and W.E. King: *Acta Mater.*, 2002, vol. 50, pp. 2599–612.
24. L.C. Lim and R. Raj: *Acta Metall.*, 1984, vol. 32, pp. 1177–81.
25. V. Randle: *Acta Mater.*, 1999, vol. 47, pp. 4187–96.
26. V. Randle: *Scripta Mater.*, 2001, vol. 44, pp. 2789–94.
27. D.M. Saylor, B.S. El-Dasher, and B.L. Adams: *Metall. Mater. Trans.*, 2004, vol. 35A, pp. 1981–89.
28. T. Watanabe: *Text. Microstr.*, 1993, vol. 20, pp. 195–216.
29. S. Tsurekawa, S. Nakamichi, and T. Watanabe: *Acta Mater.*, 2006, vol. 54, pp. 3617–26.
30. V. Randle: *The Role of the Coincidence Site Lattice in Grain Boundary Engineering*, The Institute of Materials, London, 1996, p. 46.
31. S.L. Lee and N.L. Richards: *Mater. Sci. Eng. A*, 2005, vol. 405, pp. 74–85.
32. Q. Li, B.M. Guyot, and N.L. Richards: *Mater. Sci. Eng. A*, 2007, vol. 458, pp. 58–66.
33. L. Tan and T.R. Allen: *Metall. Mater. Trans. A*, 2005, vol. 36A, pp. 1921–25.
34. P. Davies and V. Randle: *Mater. Sci. Technol.*, 2001, vol. 17, pp. 615–26.